Journal of Non-Crystalline Solids 382 (2013) 57–65

Effect of magnesium ion incorporation on the thermal stability, dissolution behavior and bioactivity in Bioglass-derived glasses

Marina T. Souza [a,*], Murilo C. Crovace [a], Cornelia Schröder [c], Hellmut Eckert [b,c], Oscar Peitl [a], Edgar D. Zanotto [a]

[a] Vitreous Materials Laboratory, Department of Materials Engineering, Universidade Federal de São Carlos — UFSCar, São Carlos, SP, Brazil
[b] Physics Institute, Universidade de São Paulo — USP, São Carlos, SP, Brazil
[c] Institut für Physikalische Chemie, WWU Münster, Corrensstrasse 30, D-48149 Münster, Germany

ARTICLE INFO

Article history:
Received 15 May 2013
Received in revised form 23 September 2013
Available online xxxx

Keywords:
Bioactive glass;
Bioactivity;
Crystallization;
Nuclear magnetic resonance

ABSTRACT

There is a strong discrepancy in the literature regarding the effect of magnesium on bioactive glasses. Hence the present study is focused on the physical and chemical behavior of the "golden standard" 45S5 glass and magnesium-containing bioactive glasses developed here to evaluate their reactivity and *in vitro* bioactivity. The aim of this study was to analyze the influence of CaO replacement by MgO, especially its effect on the rate of formation of the apatite-like layer at the glass surface, the reaction kinetics between the glasses and simulated body fluid (SBF-K9) and on the glass stability against devitrification during heating. Five melt-derived bioactive glasses of the system $24.3Na_2O–26.9(xCaO-(1-x)MgO)–46.3SiO_2–2.5P_2O_5$ ($x = 1$; 0.875; 0.75; 0.625 and 0.5) were synthesized with CaO progressively replaced by MgO. Their thermal stability on heating was characterized by DSC analysis. Their degradation and ability to form an apatite-like layer were evaluated through *in vitro* tests by immersion in SBF-K9; FTIR, ion selective electrode analysis and by solid state nuclear magnetic resonance (NMR) spectroscopy. Our results indicate that magnesium plays an important role in the stability of this glass family, defined as the difference between the glass transition temperature T_g and crystallization temperature T_x. The lower T_g observed in the MgO-rich glasses and insignificantly changed solubilities, as well as the ^{29}Si NMR results suggest that in this glass system MgO does not act as a network intermediate or former oxide, but as network modifier, as we expected. Dissolution kinetics, FTIR, and solid state ^{31}P and ^{1}H MAS-NMR consistently indicate that partial replacement of CaO by MgO in the bioglass does not influence the rate at which the initial amorphous calcium phosphate (ACP) layer is precipitated when the glass is exposed to SBF. In contrast it greatly reduces the rate of conversion of this precursor phase to the crystalline hydroxycarbonate apatite (HCA)-layer.

1. Introduction

In 1969, Hench et al. [1] found that certain glass compositions have the ability to form a chemical bond with living tissues, including hard tissues, such as bone and teeth. Since then, this class of glasses has been classified as bioactive glasses [1]. The first developed and most known bioactive glass is Bioglass® 45S5 [2]. This glass has an approximate composition of 46.3 SiO_2, 24.3 Na_2O, 26.9 CaO and 2.5 P_2O_5 (mol%). It has been tested and clinically used over several years demonstrating very satisfying results as bone graft substitute due to its osteoconductive and osteoinductive nature [3]. The bone-bonding ability of bioactive glasses is attributed to the formation of a biologically active apatite-like layer at the glass surface (when in contact with blood plasma or saliva), with composition and structure similar to that of the mineral phase of bone [1]. Several mechanisms have been proposed to explain their bioactive behavior. Currently, the most accepted one is associated with the proposals of Hench and Clark [1,4] and Kokubo et al. [5–7], who developed an *in vitro* analysis based on an acellular solution that mimics the ionic content of the blood plasma, *i.e.* SBF-K9 (Simulated Body Fluid). The interaction between the bioactive glass surface and this solution initiates the formation of a silica hydrogel layer and this layer allows the subsequent ionic precipitation and crystallization of an apatite-like phase. Nonetheless, the dissolution kinetics and the velocity of the apatite-like layer formation depend on many variables, such as glass chemical composition, surface topography, glass structure and how it interacts with the surrounding medium [8–10].

The majority of bioactive glasses have quite complex multicomponent compositions and many researchers worldwide are still aiming to improve their chemical–physical and biological properties by modifying their formula (and hence their structure). Thus, reaching an understanding of the individual function of each component in these systems is not a simple, but a truly important task. As there is some controversy in the literature (discussed in the next session) regarding the effect of Mg, the present study is thus focused on the physico-chemical behavior

* Corresponding author.
E-mail addresses: marina.trevelin@gmail.com (M.T. Souza), murilocc@yahoo.com.br (M.C. Crovace), c_schr21@uni-muenster.de (C. Schröder), eckert@ifsc.usp.de (H. Eckert), opeitl@ufscar.br (O. Peitl), dedz@ufscar.br (E.D. Zanotto).

0022-3093/$ – see front matter © 2013 Elsevier B.V. All rights reserved.
http://dx.doi.org/10.1016/j.jnoncrysol.2013.10.001

of pure 45S5 and magnesium-containing glasses to evaluate their reactivity and *in vitro* bioactivity.

Magnesium has been reported to play a relevant role in human bone growth, maintenance and repair by stimulating osteoblast proliferation [11]. Additionally, this element is involved in over three hundred chemical reactions in the human body, one of them being the regulation of calcium transport [12]. However, its function in bioactive glass formulations has been subject to conflicting explanations, mainly related to the different roles that have been attributed to this element on the glass structure. Several researchers claim that Mg is a modifier element [13,14] whereas others affirm that it can appear partly as an intermediate oxide, entering the silicate network as MgO_4 tetrahedral unit [11,12].

There are several models for the role of each element in the glass structure. Zachariasen and Sun classified magnesium as a modifier element. However, Dietzel, as early as in 1942, calculating the field strength "*F*" ($F = Z_c/a^2$; being Z_c the cation's valence and *a* the ionic radii plus the oxygen ion in Å units) classified elements with 0.1 to 0.4 field strength as network modifiers and elements with 0.5 to 1.1 as intermediates. Magnesium plays an interesting role in this classification since its ionic field strength is 0.45 falling on the borderline between network modifier and intermediate oxide [15].

A comprehensive review on magnesium containing bioactive glasses for biomedical applications has been given recently [16]. Some *in vitro* studies have shown that MgO hinders mineralization of the apatite-like layer [17–19]; for example by decreasing the thickness of the mineralized surface layers [19]. In contrast, others suggest that its presence does not affect this layer formation and even promote its *in vitro* establishment by facilitating the early stages of mineralization [20–22]. Furthermore, some studies suggest that substitution of CaO by MgO in the composition of silicate glasses would modify their stability against crystallization and improve some mechanical properties of these glasses [23]. Addition of an element such as magnesium, which has high physiological interest in the biomedical field, may be used to tailor some physico-chemical and physiological properties of bioactive glasses. Also, its presence in the glass could allow the manufacture of different products, such as scaffolds, fibers, 3D devices, *etc.*, since its addition is known to decrease the *liquidus* temperature, viscosity and sometimes the crystallization rates in some silicate glasses [14,19]. Thus, the clear establishment of the influence of Mg on the properties requires a systematic study of Mg-containing bioactive glasses.

Our findings show that the presence of magnesium decreased T_g values, increased T_x and did not cause alterations on glasses solubility and formation of an ACP layer, however, greatly delayed the crystallization of HCA.

2. Experimental

2.1. Preparation of the glasses

The reference composition in this study is the golden standard 45S5 Bioglass® invented by Hench. Five different compositions in the system $24.3Na_2O–26.9(xCaO-(1-x)MgO)–46.3SiO_2–2.5P_2O_5$ (x = 1; 0.875; 0.75; 0.625 and 0.5) were made with gradual replacement of calcium oxide by magnesium oxide. The compositions of pure and Mg-doped glasses are shown in Table 1. All the glasses were prepared using reagent grade chemicals (SiO_2, Na_2HPO_4, $CaCO_3$, Na_2CO_3, and MgO). The compositions were melted in platinum crucibles at 1450 °C for 4 h; the melts were rapidly quenched by splat cooling, which was carried out pouring the liquid between two metal plates kept at room temperature. The melting/cooling procedure was repeated for five times aiming at a more homogeneous glass. Cylindrical samples of 12 mm in diameter and 30 mm in height were cast by pouring the melt into graphite molds. The samples were annealed for 6 h at approximately 50 °C below the glass transition temperature of each composition, in a muffle furnace programmed to cool down to room temperature at 5 °C/min.

Table 1
Glass compositions of the magnesium substituted glasses in mole %.

Glass ID	SiO_2	Na_2O	CaO	MgO	P_2O_5
45S5 (x = 1)	46.3	24.3	26.9	0	2.5
F1 (x = 0.875)	46.3	24.3	23.5	3.4	2.5
F2 (x = 0.75)	46.3	24.3	20.2	6.7	2.5
F3 (x = 0.625)	46.3	24.3	16.9	10	2.5
F4 (x = 0.5)	46.3	24.3	13.45	13.45	2.5

2.2. Differential scanning calorimetry (DSC)

The glasses were characterized by DSC using a NETZSCH DSC 404 apparatus. Both reference and sample were contained within platinum crucibles. Monolithic samples of approximately 1.5 × 1.5 × 1.5 mm were prepared and then heated from room temperature to 1200 °C, at a heating rate of 10 °C/min. The glass transition temperatures (T_g) and onset crystallization temperatures (T_x) were then obtained from the corresponding DSC traces.

2.3. Nuclear magnetic resonance (NMR)

The ^{29}Si MAS-NMR spectra were recorded on a Bruker Avance 300 spectrometer at 59.595 MHz with a 7 mm rotor at a spinning speed of 4.0 kHz. 56 scans were accumulated with 90° pulses of 8.5 μs length and a relaxation delay of 3000 s. Such long relaxation delays were found to be essential for ensuring quantitative detection of all the silicon species present. Chemical shifts are reported relative to tetramethylsilane used as an external reference standard.

The ^{31}P MAS-NMR spectra of the glasses were recorded on a Bruker CXP-200 spectrometer at 80.961 MHz with a 4 mm rotor operated at a spinning speed of 10 kHz, 592 scans were accumulated with 90° pulses of 4.8 μs length and a relaxation delay of 180 s. For the samples 45S5, F2 and F4, additional NMR studies were taken on the biomineralized layers, which were removed with a razor blade after 16 h and 8 days exposure to the SBF. ^{31}P MAS-NMR measurements on those samples were conducted on a Bruker DSX-500 spectrometer at 202.49 MHz, using a 2.5 mm MAS-NMR probe operated at a 25.0 kHz spinning speed. 60 scans were accumulated at a recycle delay of 200 s. Chemical shifts are reported relative to 85% H_3PO_4 used as an external reference standard. ^1H MAS-NMR spectra on the biomineralized layers were measured at 500.13 MHz, using a Bruker DSX-500 spectrometer equipped with a 2.5 mm probe, which was operated at a spinning frequency of 25.0 kHz. 64–128 rotor synchronized Hahn spin echoes were accumulated at a recycle delay of 2 s. Chemical shifts are reported relative to tetramethylsilane used as an external reference standard.

2.4. In vitro tests

The *in vitro* tests were conducted according to Kokubo's method [24], using SBF-K9 solution.

Samples were cut into cylinders of approximately 7 mm height and 12 mm diameter and then polished with a 400-grit silicon carbide paper. All samples were rinsed and cleaned with isopropyl alcohol solution in an ultrasonic cleaner for 20 min. Then, the samples were immersed in SBF-K9 solution and placed into a sealed polyethylene bottle with a glass surface area to volume ratio of 0.1 cm^{-1} [25]. They were maintained at 37 °C during 4, 8, 16 h and 1, 2, 4, 8 and 16 days.

The *in vitro* bioactivity and chemical durability were evaluated by studying ionic exchanges between the glass samples and the solution. The elemental concentrations of Na, Ca, Mg and P in the SBF-K9 solution after soaking the pure and doped glasses were determined by an ion selective electrode (Cobas, b121 System — Roche) using ion-selective

electrodes sensitive to each species of interest, for times ranging from 4 to 16 days.

2.5. FTIR spectroscopy

The chemical changes on the glass surfaces were followed by Fourier Transform Infrared Spectroscopy (FTIR) (Perkin Elmer, Spectrum GX, DE). Spectra were obtained between 1500 and 400 cm^{-1} wave number for all samples.

2.6. Scanning electron microscope (SEM)

SEM (FEG, Phillips/FEI Company, Phenom) analyses to evaluate the bioactive glass surface degradation and formation of apatite after 24-h exposure to SBF-K9 solution were conducted for all samples.

3. Results and discussion

3.1. Differential Scanning Calorimetry (DSC)

The obtained DSC curves are shown in Fig. 1. It is possible to observe heat capacity changes associated with the glass transition at around 500–560 °C and exothermic processes associated with crystallization between 690 and 1000 °C.

The values presented in Table 2 indicate that the gradual substitution of CaO for MgO results in a decrease in the glass transition temperatures (T_g). This phenomenon may be attributed to the mixed cation effect, which is known to significantly reduce viscosity especially at low temperatures [14,19,26,27].

Table 2 also shows that the glass stability defined as [28]:

$$K_2 = T_x^h - T_g \quad (1)$$

where T_x^h the onset crystallization temperature on heating increases with increasing extent of Ca/Mg substitution.

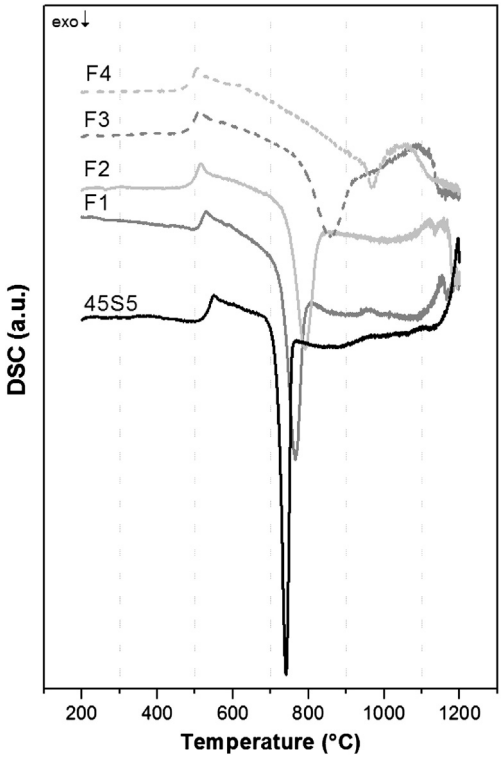

Fig. 1. DSC traces for the magnesium substituted series of glasses with increasing magnesium content from F1 to F4. Monolithic pieces of about 20 mg.

Table 2
T_g, T_x, and K_2 of the 5 glasses (with an uncertainty of about 2–3 °C).

Glass ID	T_g	T_x	K_2
Bioglass 45S5	520 °C	700 °C	180 °C
F1	505 °C	710 °C	205 °C
F2	485 °C	735 °C	250 °C
F3	480 °C	785 °C	305 °C
F4	475 °C	945 °C	470 °C

Also according to Fig. 1, the onset crystallization temperature (T_x) increases linearly and the peaks are less pronounced with increasing Mg content. This could be attributed to stronger Si–O–Mg compared to the Si–O–Ca bonding interaction [14], attributable to the higher ion potential (charge/radius ratio) of the Mg^{2+} ions.

Most authors affirm that combeite ($Na_2Ca_2Si_3O_9$) would result as the main crystalline phase after heat treatment of Bioglass 45S5 [25,29,30]. Recently, Lefebvre et al. [31] and Fagerlund and Hupa [32] suggested that $Na_2CaSi_2O_6$ would be the major crystalline phase instead of $Na_2Ca_2Si_3O_9$, but this discrepancy can be partially explained by the solid solubility of the three oxides [33]. However, regardless of the real stoichiometry of the crystals formed during heat-treatment of Bioglass 45S5, magnesium addition probably hinders the formation of this calcium sodium silicate phase.

The overall crystallization process is affected by the CaO/MgO replacement since the latter promotes mixed cation effects, which may decrease the diffusion coefficients of the different ions present in the glass structure [14].

3.2. In vitro tests — changes in the SBF composition

Immersion of any bioactive glass in SBF-K9 solution leads to dissolution of all the ions present in these materials, mainly Si, Na, Ca and P. In this study Mg was also analyzed. Therefore, understanding the kinetic reactions of these elements with this synthetic fluid calls for special attention, since they are directly involved in the formation of the apatite-like layer.

The cumulative variation of Na, Ca, Mg, and P ionic concentrations with soaking time in SBF is shown on Fig. 2. The quantity of Mg rises with time in all cases; and as the Mg content in the glass composition is increased, a greater amount of Mg is released into the solution.

The P concentration in the solution decreases continuously with time, which may be attributed to the concomitant development of the Ca–P rich layer.

The Ca concentration reaches a minimum after the first hours of immersion and then gradually increases up to 16 days. As can be observed, the lower the Ca content in the glass compositions, the lower is the increase of Ca in the SBF solution, except for 45S5, for which the Ca concentration does not change significantly until the end of the test. The increase of Ca concentration after 24 h may be attributed to the depletion of P in the solution, as can be observed in Fig. 2b, hence the Ca leached to the solution would react only with a small quantity of P also leached from the glass. Thus, the majority of the Ca ions are not able to precipitate and form more of the amorphous calcium phosphate (ACP) layer. Also for 45S5 samples the formation of a hydroxy carbonate apatite (HCA) layer leads to stabilization of the Ca quantity present in the SBF-K9 solution, while for the other compositions the formation of HCA is delayed and thus rising Ca concentrations are observed with time.

The Na concentration increases with time for all compositions. The magnesium doped glass series (F1 to F4) demonstrate the highest values for this element in the final periods of analysis. Based on previous studies [22,34], this fact could be attributed to the faster rate of silica-gel layer formation for compositions containing magnesium.

Several studies affirm that the silica gel thickness increases with increasing Mg content in the glass [22,23,34,35]. This indicates that

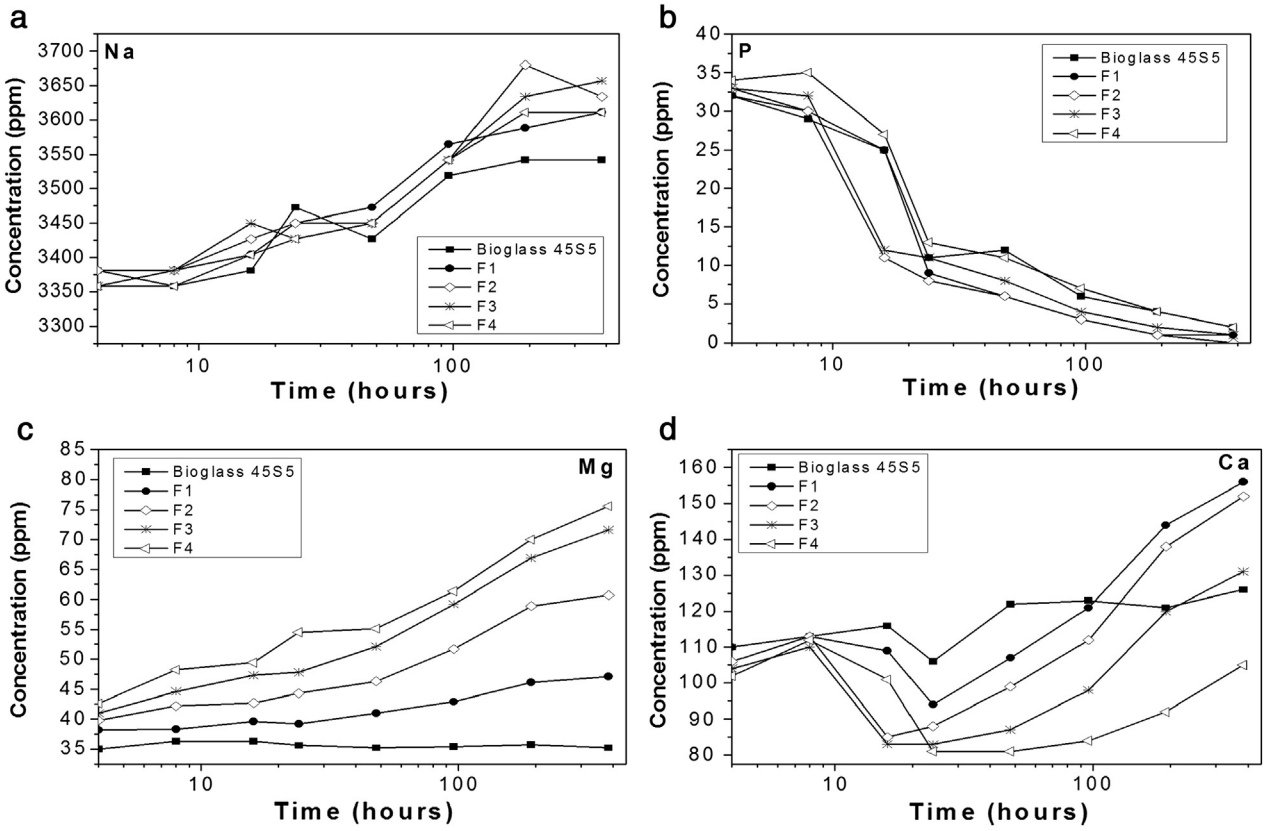

Fig. 2. Elemental concentrations in SBF solution after immersion of glass specimens with different MgO content for times between 4 and 384 h.

the reactions involved in the Stages I and II, proposed by Hench [1], are accelerated in the compositions with higher Mg content, consequently, a faster leaching of Na is expected.

The pH of the SBF solutions increases with time and with increasing magnesium content in the glass for each soaking time (Fig. 3). This increase can be attributed to the increase of Ca and Mg levels that are continuously leached into the solution and are not yet incorporated in the precipitated apatite layer.

It is important to observe that for this glass series the amount of Ca + Mg %-mol was kept constant, as well as Si and P.

Fig. 4 shows the sum of these two elements [Ca + Mg] leached to the solution during the *in vitro* tests.

In the first periods of analysis all glasses show a very similar trend. There is an increase of leaching for these two elements followed by a decrease in the 24 h analysis. However, after 48 h the value for Bioglass 45S5 [Ca + Mg] does not change significantly with time, whereas for the other glasses these [Ca + Mg] concentrations tend to increase further. However, it is possible to observe that the amount obtained for this sum decreased with the increase of magnesium content in the glass, even though these glasses present much higher values when compared to Bioglass 45S5.

The stability obtained for Bioglass 45S5 may be attributed to the continued formation and crystallization of the apatite-layer, whereas for the other glasses the presence of magnesium inhibits the transformation

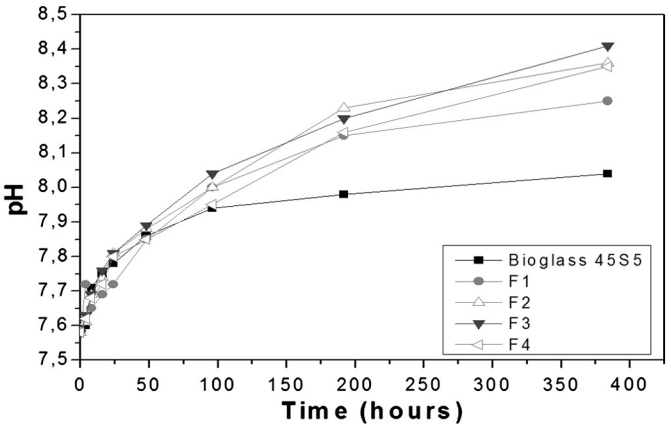

Fig. 3. pH of SBF solution after immersion of glass specimens with different MgO content for times between 4 and 384 h.

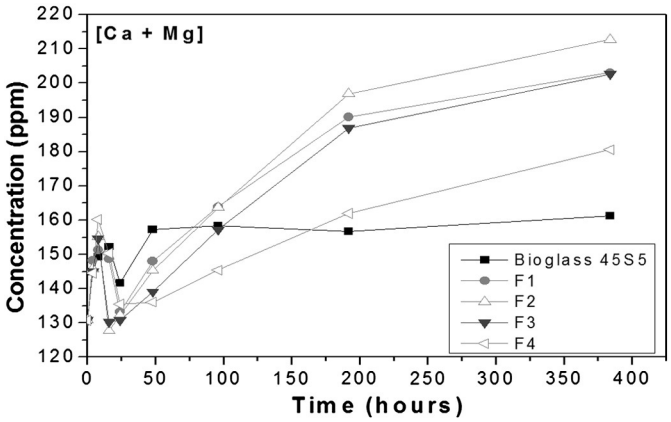

Fig. 4. (Ca + Mg) concentrations in SBF solution after immersion of glass specimens with different MgO content for times between 4 and 384 h.

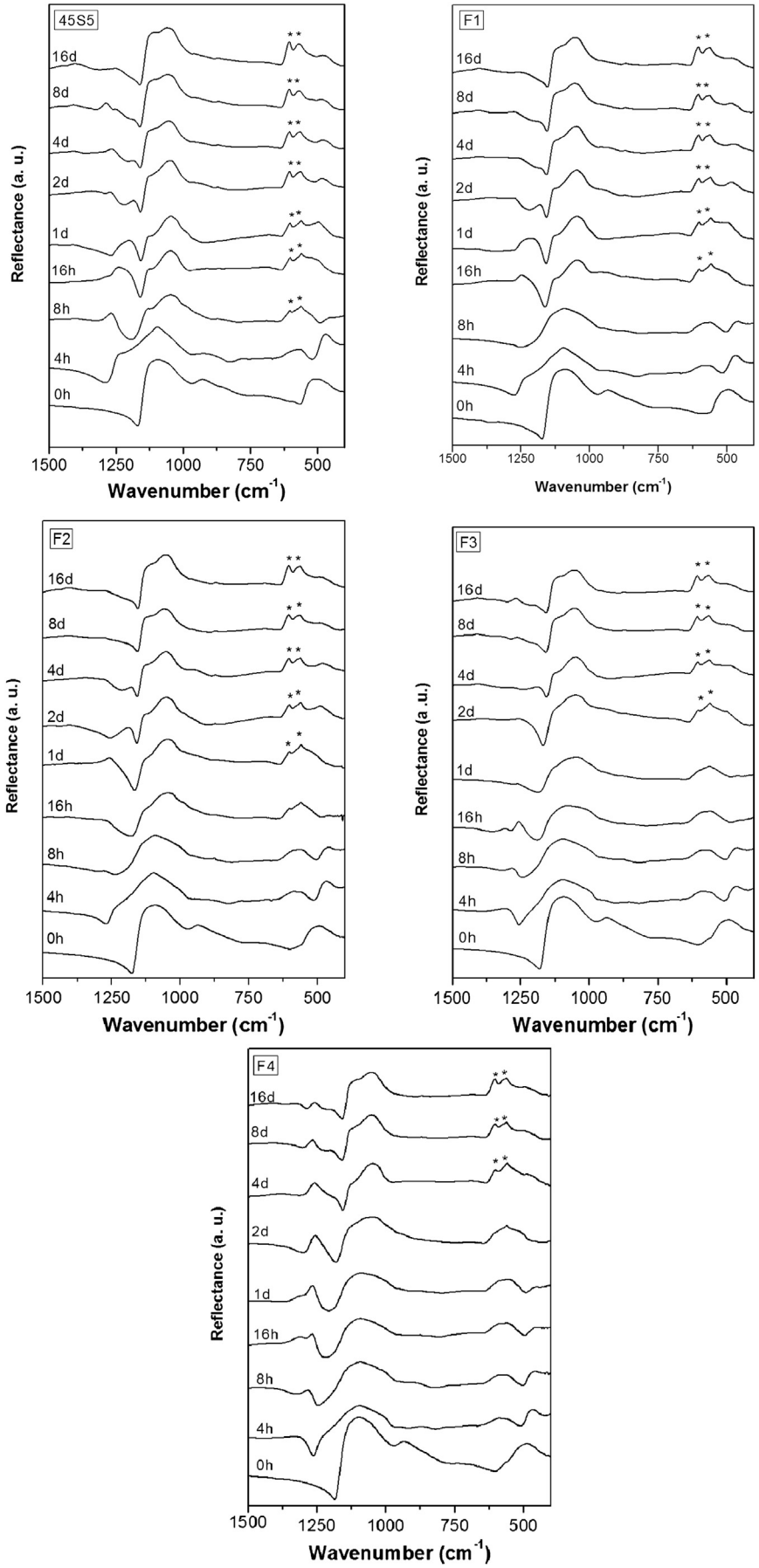

Fig. 5. FTIR spectra of 45S5 and F1 to F4 for immersion times between 4 and 384 h; (*) hydroxycarbonate apatite.

of ACP into HCA. In these glasses the presence of a more open amorphous structure allows a further leaching of the ions from the glass.

Kibalcyc et al. [36] affirm that the presence of magnesium in a solution does not change the solubility of phases such as amorphous calcium phosphate (ACP) and octacalcium phosphate (OCP); instead it only delays the transformation of the ACP phase to a crystalline material and inhibits growth of OCP, but not the nucleation of this phase.

Several authors claim that when the amorphous phosphate phase precipitates it incorporates some magnesium, whose quantity is related to its concentration in the SBF solution [37–39]. Depending on the amount incorporated, a structural mismatch occurs in the pre-nucleated structures of hydroxyapatite (HA), and thus this phase cannot properly develop.

Another mechanism proposed for this delay of HA formation is the poisoning of the surface of HA nuclei by magnesium or some of its complexes. This poisoning supposedly occurs when the magnesium ions are adsorbed into the active growth sites, retarding or inhibiting the crystal growth of HA [37,38,40].

Shimabayashi et al. [41] showed that the cation binding affinity to HA follows the order $Ca^{2+} > Ba^{2+} > Mg^{2+}$; dislocations on HA and Ca defects being their binding sites. They also affirm that this cation adsorption to HA can increase the positive charge on the surface influencing the dispersion properties of HA, such as sedimentation volume and mean diameter of the HA particles.

Abbona and Baronnet [42] also affirmed that magnesium additions cause strong effects on apatite nucleation, crystal morphology, crystal perfection and growth kinetics. Its presence reduces the size and structure of the amorphous calcium phosphate particles and generates particles smaller and more irregular in shape and richer in defects.

3.3. Apatite-like layer formation (FTIR)

Fig. 5 shows the infrared spectra of the precipitates formed on the glass surfaces after 4, 8, 16 h and 1, 2, 4, 8 and 16 days in SBF. Bands were assigned on the basis of published data according to Peitl et al. [43].

The presence of two peaks approximately at 610 and 560 cm^{-1} indicates that the apatite-layer (HCA) is well formed and crystallized after 8 h for 45S5 Bioglass. The soaking time required until this phase is observed increases as calcium is successively substituted by magnesium. F4 samples only present these two peaks after 96 h (4 days) of immersion in SBF solution. After 48 h, peaks between 540 cm^{-1} and 415 cm^{-1} (Si–O–Si) are not detected, indicating that at this stage the silica-rich layer is covered by an ACP layer.

Vallet-Regí et al. [23] affirm that this delay on the formation of the apatite-like layer in glasses of the $CaO–MgO–SiO_2–P_2O_5$ system may be attributed to two main effects. The first one involves the decrease of the solubility of the glass, since Mg-O chemical bonds are stronger than Ca–O bonds [14]. The second one refers to the influence of the Mg on the rate of precipitation of the amorphous calcium phosphate layer in SBF. This element, when leached to the SBF solution, decreases the rate of formation of a more stable apatite phase [11,23].

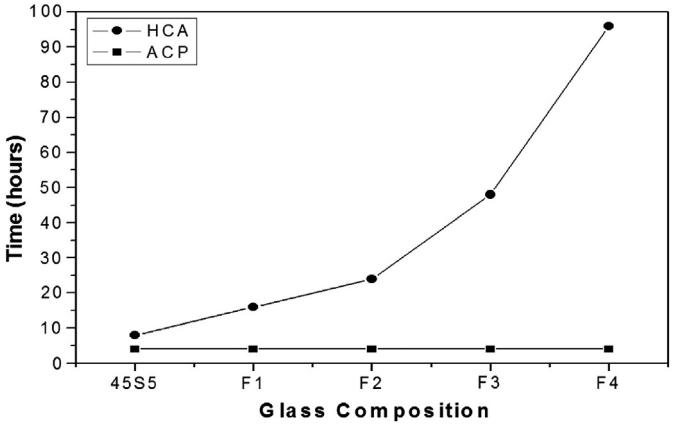

Fig. 6. Time required for the ACP and the apatite-like layer formation for different glass compositions.

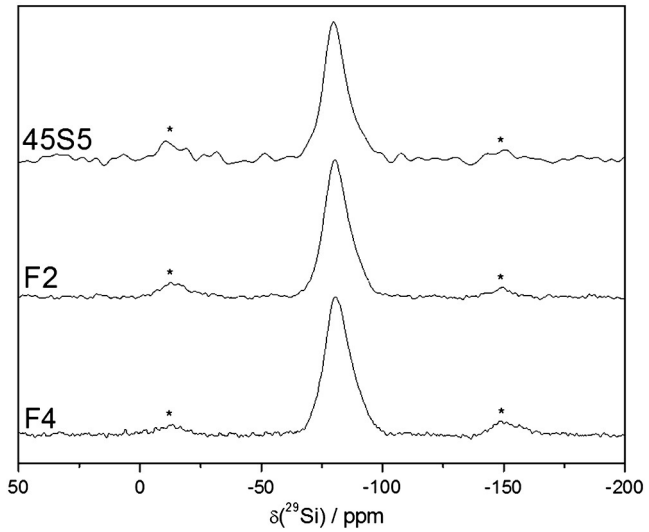

Fig. 7. ^{29}Si MAS NMR spectra of 45S5, F2 and F4 glasses. Spinning sidebands are indicated by asterisks.

It is also known that, in most cases, the leaching rate of alkaline-earth ions from a silicate glass decreases with decreasing ionic radius [22]. Hence a reduction of the rate of apatite-like layer formation is expected as the Mg content is increased.

In Fig. 6 it is possible to compare the onset time for the ACP layer and the apatite-like layer (HCA) formation on the sample surfaces. Although the time range between measurements was large, the higher the magnesium content, the higher is the time needed to the formation and crystallization of the apatite-layer, while the time required for ACP formation for all samples was practically the same. This finding indicates that the (probably) reduced glass solubility has no significant influence on the formation of this amorphous layer (ACP).

3.4. Nuclear magnetic resonance (NMR) of the bulk samples

Fig. 7 shows ^{29}Si MAS-NMR spectra of 45S5, F2 and F4 glasses. With increasing Mg content, the curve shapes become slightly more asymmetric, indicating an increasing contribution from a low-frequency

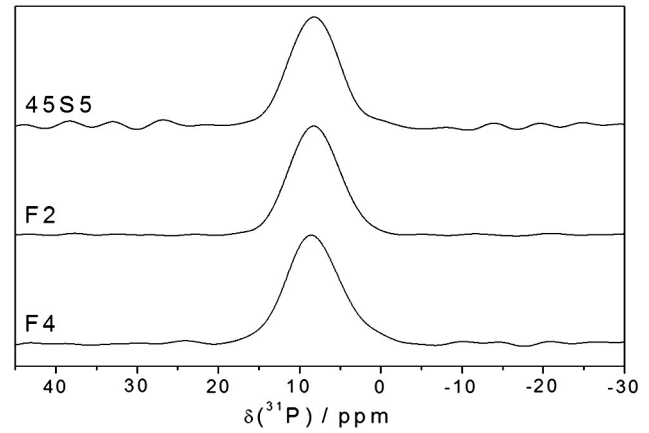

Fig. 8. ^{31}P MAS NMR spectra of 45S5, F2 and F4 glasses.

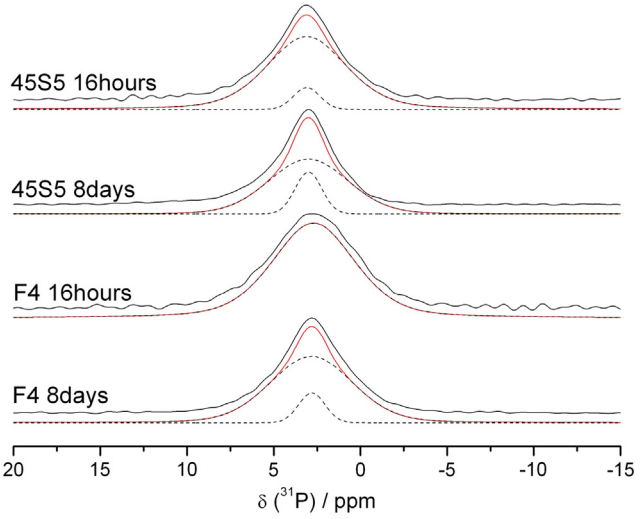

Fig. 9. ^{31}P MAS-NMR spectra of samples 45S5 and F4 after different exposure times. Red curves depict a simulation based on the two individual components (dashed curves) assigned to ACP (broad component) and HCA (sharp component).

shoulder, presumably arising from Si-atoms in the vicinity of Mg^{2+} ions. However, the spectroscopic resolution is insufficient for attempting a reliable deconvolution of these lineshapes. The rather subtle changes of the center of gravity from −80.7 ppm in 45S5 to −82.0 ppm in F4 observed in the present study are somewhat in contrast to those of Oliveira et al. [13] who suggest that Mg acts in the role of a network former species, resulting in the formation of tetrahedral $MgO_{4/2}^{2-}$ units, which redirect the network modifier cations such as Na^+ and thereby promote a re-polymerization of the silicate network. The spectra of the present materials do not give evidence of such a mechanism.

Fig. 8 shows the corresponding ^{31}P MAS-NMR spectra. Aside from slight variations in the line positions and widths, which are, however, close to the experimental error limits, the spectra in Fig. 8 suggest that the species giving rise to this signal near 8.2 ppm are essentially identical. They indicate that phosphate is exclusively present in the form of $Q^{(0)}$ orthophosphate units in an amorphous environment. The increase in line width from 590 Hz in 45S5 to 660 Hz in F4 suggests a wider isotropic chemical shift distribution in the latter sample, arising from multiple phosphate environments with different numbers of Ca^{2+} and Mg^{2+} ions. No reliable statement can be made, however, regarding the Ca/Mg distribution in the vicinity of the orthophosphate species.

3.5. Solid state NMR spectra of biomineralized samples

Fig. 9 shows the ^{31}P MAS-NMR spectra of the biomineralized layers recovered from samples 45S5, F2 and F4 as described in the Experimental section. The ^{31}P MAS-NMR spectra show subtle but consistent trends as a function of composition and exposure time. They can be interpreted in conjunction with previous results from Edén and coworkers, [44–46] who followed the biomineralization of glasses with composition "S85" (10 CaO–85SiO_2–5 P_2O_5 — mol%) in SBF [44–46].

These authors showed that the ^{31}P MAS NMR spectra can be deconvoluted in terms of two distinct lineshape components [44], which can be assigned to ACP and HCA, respectively. While these two components are spectroscopically too close to be resolved on the basis of their chemical shifts, they possess quite different line widths (5.4 and 1.8 ppm, respectively). Following the procedure of these authors we simulate our spectra as superpositions of two lineshape components having the same chemical shift (near 3.0 ppm), but different line widths to estimate the percentages of ACP and HCA formed after 16 h and 8d, respectively. Table 3 summarizes the relevant

Table 3
Quantitative deconvolution analysis of the ^{31}P MAS NMR spectra in terms of the ACP and the HCA contributions.

Sample	45S5 16 h	45S5 8 days	F2 16 h	F2 8 days	F4 16 h	F4 8 days
δ(^{31}P)/ppm	3.1	3.0	3.0	2.9	2.7	2.8
FWHH/ppm ACP	5.4	5.4	6.5	5.4	5.6	5.6
FWHH/ppm HCA	1.8	1.8	–	1.9	–	1.8
% ACP/HCA	93/7	80/20	100/0	83/17	100/0	89/11

fit parameters. These results clearly confirm the conclusion from the FTIR spectra that HCA formation is considerably delayed in the Mg-containing samples. For example no HCA is detected after 16 h in either F2 or F4, and the amount of HCA formed after 8 days is only half as large in F4 as it is in 45S5. Finally, the spectra give no evidence for the formation of OCP, which would give rise to four distinct peaks in the shift range between −1 and +4 ppm [47,48]. Still, as discussed below, the ^{1}H MAS-NMR spectra suggest the presence of some OCP, possibly in a disordered form. Furthermore, as the broad peak of ACP observed here encompasses the overall shift range of the ^{31}P resonances in OCP, we cannot exclude a structural relationship between ACP and OCP on the basis of our ^{31}P MAS-NMR results.

The ^{1}H MAS-NMR spectra (see Fig. 10) are dominated by surface adsorbed water on the ACP/HCA phases (broad peak near 5.0 ppm). In addition, four distinct resonances near 1.2, 1.1, 0.8 and 0.1 ppm are observed. Contrary to the suggestion made in Ref. [48], in the present samples, these resonances cannot be attributed to organic residues, as the present materials were never exposed to organics, aside from TRIS buffer, whose resonances would occur at rather different chemical shifts. Rather, we assign these signals, which were previously observed in various octacalcium phosphate samples [48–50], as well as in nanocrystalline hydroxyapatite [51] to highly mobile water species within differently layered precursor structures preceding the formation of hydroxyapatite. We attribute these highly characteristic lines to protons in the acid phosphate/water layer of a disordered form of OCP that is forming as a precursor structure to hydroxyapatite in these samples. The disordered state of this OCP phase may be the reason that its ^{31}P MAS-NMR signals cannot be resolved in the present samples.

We further note, that in all the 16 h-samples, ^{1}H MAS-NMR features pertaining to the OCP phase are considerably less-well developed, indicating more disorder and less mobility of these water pools in the ACP phase, which is dominant at that stage of crystallization. Moreover, sample F4 shows a signal near 2.0 ppm, which can be assigned to the

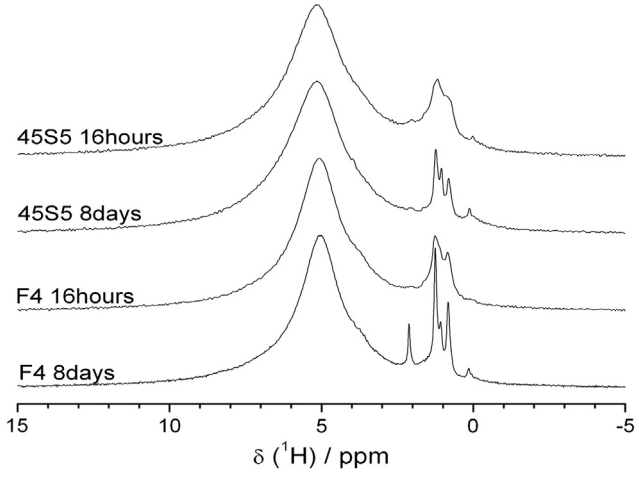

Fig. 10. ^{1}H MAS-NMR spectra obtained on the 45S5 and F4 samples after different times of exposure to SBF.

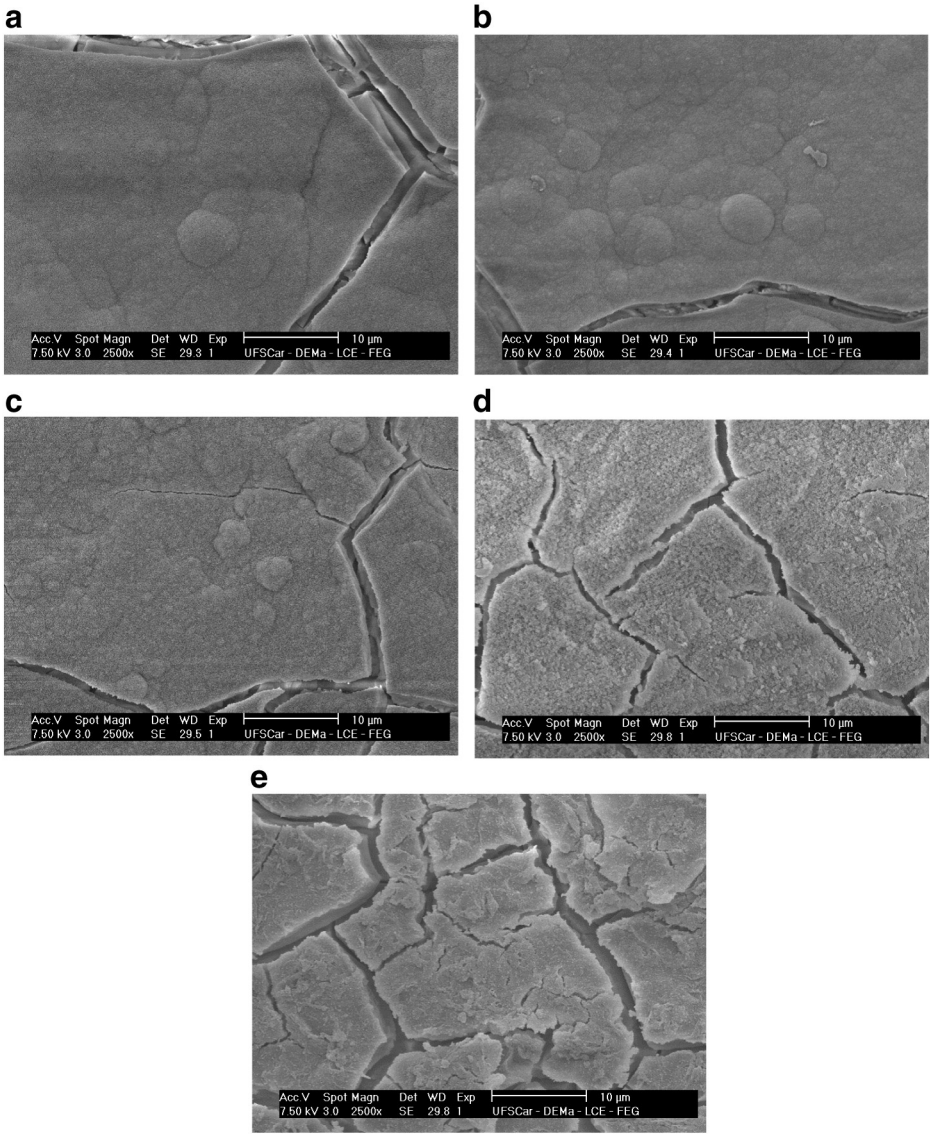

Fig. 11. SEM micrographs (×2.500) of 45S5 (a), F1 (b), F2 (c), F3 (d) and F4 (e) after a 24 h immersion in SBF-K9 solution.

silanol species of the partially hydrated silicate layer. The appearance of this peak suggests that the isolation procedure applied for the removal of the calcium phosphate containing phase was not entirely successful and part of the hydrated silicate layer was also recovered. Finally, the spectra show only a minor contribution from the OH groups of the hydroxyapatite phase (spectral intensity near 0 ppm [50]). As previously noted [44–46], the difficulty in detecting the structural hydroxyl groups in biomineralized samples *via* single-pulse ^{1}H MAS NMR must be attributed to the dominance of the surface-adsorbed water in these samples.

3.6. Scanning electron microscopy (SEM)

All other results obtained in this study and the SEM images of the specimens after 1 day soaking time (Fig. 11) allow us to affirm that formation of an apatite-layer indeed occurred on glasses 45S5 and F1 to F2. But, the globular shape pattern commonly found for apatite is not seen for F3 and F4 samples, indicating the formation of an amorphous calcium phosphate layer on their surfaces. These results indicate once more that magnesium does not affect the glass solubility, but only the crystallization of the apatite-layer in SBF.

4. Conclusions

Gradual replacement of CaO by MgO in 45S5 leads to lower values of T_g, higher T_x, and almost no change in solubility and formation of an ACP layer. However, it greatly delayed the crystallization of HA in SBF-K9 in our *in vitro* tests. The lower T_g and insignificantly changed solubilities, as well as the ^{29}Si NMR results suggest that in this glass system MgO does not act as a network intermediate oxide or former, but as a network modifier. The substantially longer time to crystallize HCA is not an effect of lower solubility, as the time for the formation of the ACP layer is independent of MgO content, but a side effect of the Mg concentration in the solution. The presence of this element in the glass or dissolved in the solution, possibly changes thermodynamic variables leading to lower nucleation and crystal growth rates of HCA from its precursor, the amorphous calcium phosphate layer.

Acknowledgements

We are thankful to Brazilian funding agencies CNPq and Fapesp for granting student fellowships, and especially to Fapesp — São Paulo Research Foundation — grant number 2013/07793-6 (CERTEV —

Center for Research, Technology and Education in Vitreous Materials) for funding this research work.

References

[1] L.L. Hench, J. Am. Ceram. Soc. 74 (7) (1991) 1487–1510.
[2] L.L. Hench, R.J. Splinter, W.C. Allen, T.K. Greenlee Jr., J. Biomed. Mater. Res. Symp. 36 (1971) 117–141.
[3] L.L. Hench, J. Wilson, Introduction, in: L.L. Hench, J. Wilson (Eds.), An Introduction to Bioceramics, World Scientific Publishing Co. Pte. Ltd., Singapore, 1993, pp. 1–24.
[4] A.E. Clark, L.L. Hench, H.A. Paschall, J. Biomed. Mater. Res. 10 (2) (1976) 161–174.
[5] T. Kokubo, J. Non-Cryst. Solids 120 (1990) 138–151.
[6] T. Kokubo, Biomaterials 12 (1991) 155–163.
[7] T. Kokubo, H. Kushitani, C. Ohtsuki, S. Sakka, T. Yamamuro, J. Mater. Sci. Mater. Med. 3 (1992) 79–83.
[8] A.J. Salinas, J. Roman, M. Vallet-Regi, J.M. Oliveira, R.N. Correia, M.H. Fernandes, Biomaterials 21 (3) (2000) 251–257.
[9] J. Roman, A.J. Salinas, M. Vallet-Regi, J.M. Oliveira, R.N. Correia, M.H. Fernandes, Biomaterials 22 (14) (2001) 2013–2019.
[10] M.M. Pereira, A.E. Clark, L.L. Hench, J. Am. Ceram. Soc. 78 (1995) 463–2468.
[11] J. Ma, C.Z. Chen, D.G. Wang, J.H. Hu, Mater. Lett. 65 (2011) 130–133.
[12] S.J. Watts, R.G. Hill, M.D. O'Donnell, R.V. Law, J. Non-Cryst. Solids 356 (2010) 517–524.
[13] J.M. Oliveira, R.N. Correia, M.H. Fernandes, J. Rocha, J. Non-Cryst. Solids 265 (3) (2000) 221–229.
[14] J.M. Fernández Navarro, El vidrio, Colección Textos Universitarios, in: J.M. Fernández Navarro (Ed.), 6, C.S.I.C., Madrid, 1991, p. 140.
[15] A.K. Varshneya, Fundamentals of Inorganic Glasses, 1st ed. Academic Press Inc., San Diego, 1994. 27–60.
[16] M. Diba, F. Tapia, A.R. Boccacchini, L.A. Strobel, Int. J. Appl. Glas. Sci. 3 (2012) 221.
[17] Y. Ebisawa, T. Kokubo, K. Ohura, T. Yamamuro, J. Mater. Sci. Mater. Med. 1 (1990) 239–244.
[18] T. Kasuga, K. Nakagawa, M. Yoshida, E. Miyade, J. Mater. Sci. 22 (1987) 3721–3724.
[19] J. Massera, L. Hupa, M. Hupa, J. Non-Cryst. Solids 358 (2012) 2701–2707.
[20] D. Pereira, S. Cachinho, M.C. Ferro, M.H.V. Fernandes, J. Eur. Ceram. Soc. 24 (2004) 3693–3701.
[21] J.S. Moya, A.P. Tomsia, A. Pazo, C. Santos, F. Guitian, J. Mater. Sci. Mater. Med. 5 (1994) 529–532.
[22] J.M. Oliveira, R.N. Correia, M.H. Fernandes, Biomaterials 23 (2) (2002) 371–379.
[23] M. Vallet-Regí, A.J. Salinas, J. Román, M. Gil, J. Mater. Chem. 9 (1999) 515–518.
[24] T. Kokubo, H. Kushitani, S. Sakka, T. Kitsugi, T. Yamamuro, J. Biomed. Mater. Res. 24 (1990) 721–734.
[25] O. Peitl, E.D. Zanotto, L.L. Hench, J. Non-Cryst. Solids 292 (2001) 115–126.
[26] A. Fluegel, Glas. Technol. Eur. J. Glas. Sci. Technol. A 48 (1) (2007) 13–30.
[27] M.B. Volf, Chemical approach to glass, Glass Science and Technology, vol. 7, Elsevier, Amsterdam, 1984, p. 594.
[28] M.L.F. Nascimento, L.A. Souza, E.B. Ferreira, E.D. Zanotto, J. Non-Cryst. Solids 351 (2005) 3296–3308.
[29] D.C. Clupper, L.L. Hench, Biomaterials 318 (2003) 43–48.
[30] A. El Ghannam, E. Hamazawy, A. Yehia, J. Biomed. Mater. Res. 55 (2001) 387–398.
[31] L. Lefebvre, J. Chevalier, L. Gremillard, R. Zenati, G. Thollet, D. Bernache-Assolant, Acta Mater. 55 (10) (2007) 3305–3313.
[32] S. Fagerlund, L. Hupa, Ceram. Mater. 62 (3) (2010) 349–354.
[33] L. Hupa, Tailoring of bioactive glasses, in: M. Ramalingam, et al., (Eds.), Tissue Engineering and Regenerative Medicine: A Nano Approach, vol. 1, CRC Press, Taylor & Francis Group, LLC, Florida, 2013, pp. 43–58.
[34] E. Dietrich, H. Oudadesse, A. Lucas-Girot, M. Mami, J. Biomed. Mater. Res. A 88 (4) (2009) 1087–1096.
[35] Y. Ebisawa, T. Kokubo, K. Ohura, T. Yamamuro, J. Mater. Sci. Mater. Med. 4 (1992) 225–232.
[36] W. Kibalczyc, J. ChristoVersen, M.R. Christo Versen, A. Zielenkiewicz, W. Zielenkiewicz, J. Cryst. Growth 106 (1990) 355–366.
[37] F. Abbona, M. Franchini-Angela, J. Cryst. Growth 104 (1990) 661–671.
[38] X. Cao, W. Harris, Environ. Sci. Technol. 42 (2) (2008) 436–442.
[39] A. Bigí, G. Faliai, E. Foresti, M. Gazzano, A. Ripamonti, N. Roveri, J. Inorg. Biochem. 49 (1993) 69–78.
[40] A.L. Boskey, A.S. Posner, Mater. Res. Bull. 9 (1974) 907–916.
[41] S. Shimabayashi, C. Tamura, M. Nakagaki, Chem. Pharm. Bull. 29 (1981) 2116–2122.
[42] F. Abbona, A. Baronnet, J. Cryst. Growth 165 (1996) 98–105.
[43] O. Peitl, G.P. LaTorre, L.L. Hench, J. Biomed. Mater. Res. 30 (1996) 509–514.
[44] P.N. Gunawidjaja, I. Izquierdo-Barba, R. Mathew, K. Jansson, A. Garcia, J. Grins, D. Arcos, M. Vallet-Regi, M. Edén, J. Mater. Chem. 22 (2012) 7214–7223.
[45] R. Mathew, P.N. Gunawidjaja, I. Izquierdo-Barba, K. Jansson, A. Garcia, D. Arcos, M. Vallet-Regi, M. Edén, J. Phys. Chem. C 115 (2011) 20575–20582.
[46] P. Gunawidjaja, A.Y.H. Lo, I. Izquierdo-Barba, A. Garcia, D. Arcos, B. Stevensson, J. Grins, M. Vallet-Regi, M. Edén, J. Phys. Chem. C 114 (2010) 19345–19356.
[47] Y.H. Tseng, J. Zhan, K.S.K. Lin, C.Y. Mou, J.C.C. Chan, Solid State Nucl. Magn. Reson. 26 (2004) 99–104.
[48] E. Davies, M.J. Duer, S.E. Ashbrook, J.M. Griffin, J. Am. Chem. Soc. 134 (2012) 12505–12515.
[49] E. Leonova, I. Izquirdo-Barba, D. Arcos, A. Lopez-Noriega, N. Hedin, M. Vallet-Regi, M. Edén, J. Phys. Chem. C 112 (2008) 5552–5562.
[50] J.P. Yesinowski, H. Eckert, J. Am. Chem. Soc. 109 (1987) 6274–6282.
[51] C. Jaeger, S. Maltsev, A. Karrasch, Key Eng. Mater. 309–311 (2006) 69–72.